 doi:10.20944/preprints202107.0370.v1

Article

Variability of Gravel Pavement Roughness: Analysis of the Impact on Vehicle Response and Driving Comfort

Vidas Žuraulis [1], Henrikas Sivilevičius [1], Eldar Šabanovič [1], Valentin Ivanov [2,*] and Viktor Skrickij [1]

[1] Transport and Logistics Competence Centre; Vilnius Gediminas Technical University, Saulėtekio al. 11, LT-10223 Vilnius, Lithuania; vidas.zuraulis@vilniustech.lt (V.Ž.); henrikas.sivilevicius@vilniustech.lt (H.S); elder.sabanovic@vilniustech.lt (E.Š.); viktor.skrickij@vilniustech.lt (V.S.)

[2] Automotive Engineering Group, Technische Universität Ilmenau, Ehrenbergstr. 15, 98693 Ilmenau, Germany; valentin.ivanov@tu-ilmenau.de (V.I.)

* Correspondence: valentin.ivanov@tu-ilmenau.de;

Featured Application: The article presents the methodology for adaptation of pavement quality indexes for gravel pavement. The findings presented in the article can be used to improve driving safety and gravel pavement maintenance.

Abstract: The gravel road pavement has a lower construction cost but poorer performance than the asphalt surface. It also emits dust and deforms under the impact of vehicle loads and ambient air factors. The resulting ripples and ruts are constantly deepening, increasing vehicle vibrations and fuel consumption, reducing safe driving speed and comfort. In this article, existing pavement quality evaluation indexes are analysed, and a methodology for their adaptation for roads with gravel pavement is proposed. This article reports the measured wave depth and length of the gravel pavement profile by the straightedge method of a 160 m long road section in three road exploitation stages. The measured pavement elevation was processed according to ISO 8608, and vehicle frequency response has been investigated using simulations in MATLAB/Simulink. The applied International Roughness Index (IRI) analysis showed that a speed of 30-45 km/h instead of 80 km/h provides the objective results of IRI calculation on the flexible pavement due to a decreasing velocity of vehicle's unsprung mass on a more deteriorated road pavement state. The influence of the corrugation phenomenon of gravel pavement has been explored, identifying specific driving safety and comfort cases. Finally, an increase in the Dynamic Load Coefficient (DLC) at a low speed of 30 km/h on the most deteriorated pavement and a high speed of 90 km/h on the middle-quality pavement demonstrates the demand for timely gravel pavement maintenance and the complicated prediction of a safe driving speed for drivers.

Keywords: gravel pavement; roughness; straightedge; power spectral density; international roughness index; vehicle response; driving comfort

1. Introduction

The pavements of road and urban street are mostly made of concrete, asphalt, cobblestone and gravel. The share of gravel pavements, particularly on local and regional roads of low and middle-income countries, remains relatively significant. Decreased handling, comfort, impact on roadside areas and other destructive indicators from this point of view make the global sustainable transportation hardly achievable [1]. The costs of gravel pavement construction are the lowest; however, its strength, environmental impact and driving conditions are the worst [2,3,4]. Such pavement must be maintained continuously by reducing the transverse ripples' resulting height and employing the blading technique. The gravel pavement also needs to fill with additional bulk material periodically due to the deterioration process. Rough gravel pavement increases fuel consumption and gas emissions [5], which is incompatible with people's mobility and life quality needs and

 doi:10.20944/preprints202107.0370.v1

environmental principles. It is estimated that taking a temporal reference of 25 years, paving 1 km of gravel roads results in 230,000 litres of fuel saved and 580 tons of CO2 emissions avoided [6]. Moreover, many road accidents occur on gravel roads with relatively high traffic volume [7]. Finally, safety, stability and comfort systems including suspension development must also be adapted to operate efficiently under an imperfect pavement having different roughness levels [8,9,10,11,12,13,14].

Currently, there are no straightforward methodologies to determine the gravel road surface condition according to the driver's need to travel safely and comfortably. The existing research of vehicle response analysis, safety, durability, and fatigue loads are mostly related with paved roads [15,16,17,18]. Different indexes are used for road pavement quality evaluation; however, they are mainly used for asphalt or concrete. One of the approaches of this research is to analyse existing indexes and develop a methodology for their adaptation for roads with gravel pavement. Instead of developing an original index, a modification of a widely used one is proposed, thus increasing the possibility of its further usage by operators ensuring road quality and other researchers.

The goal is to develop the methodology for gravel road quality evaluation concerning pavement deterioration and vehicle dynamics response, providing appropriate maintenance indication for this pavement type.

The paper has five sections, including an introduction. In Section 2, related works about the road roughness are analysed, the specificity of the gravel pavement is provided. Such road impact on vehicle dynamics considering comfort and handling, vehicle components degradation is taken into account. Road roughness measurement techniques and indexes used for quality evaluation are reviewed; the methodological gaps are identified. In Section 3, the research strategy is provided. Also, the theoretical background for the selected index calculation is presented. In Section 4, the experimental procedure is described. In Section 5, the specificity of the International Roughness Index (IRI) approach for the gravel pavement is analysed, and vehicle dynamics response in the context of the excitation of sensitive frequencies at different driving speeds on the gravel pavement is examined. The conclusions summarise the main results and explain how IRI can be used for quality evaluation of gravel pavements and define future research guidelines.

2. Related works

Three classes of the grouped road pavement roughness parameters, including geometric road parameters, statistical values, and performance-based indicators, are usually used in literature [19]. Statistical parameters of geometric characteristics are directly related to the pavement texture profile's geometry, which is described in international standard ISO 13473-2 [20]. The performance indicators describe tyre – surface interaction, and this area are related to a broad scope of vehicle dynamics aspects.

Rapid changes in the surface characteristics are one of the gravel pavement's specific properties. The deterioration of gravel pavement is affected by climatic and meteorological factors such as wind, water, and temperature fluctuations. These factors alone or in combination with vehicle loads break down the gravel pavement even faster. Thus, a five-level rating system has been introduced to evaluate the pavement surface of gravel roads [21], it includes: i) crown (shaping and grading quality); ii) drainage (roadside ditches and culverts); iii) gravel layer (thickness, gradation, particles shape and regularity, gravel durability); iv) surface deformation (corrugation, potholes, ruts); v) surface defects (dust, loose of aggregate particles). The deteriorated pavement having the specific waves of a narrow band spectrum is partly similar to the rigid pavement containing a high number of cosine shape obstacles. In such a case, the road profile is considered as quasi-homogeneous, i.e. standard profile processing is not directly applicable [22].

The corrugation or 'washboard' phenomenon for gravel pavement occurs in small transverse ripples. The vehicle wheel's periodical vertical motion caused by suspension characteristics and body bounce affects harmonic loads and ripples' formation. Very small and initially insignificant imperfections primarily cause the corrugation on the unpaved

 doi:10.20944/preprints202107.0370.v1

road, such as little undulation, the variance of surface flexibility or even sporadic grains [23,24]. Following a study on the factors causing gravel road corrugation, regression analysis enabled the researchers to define the extent of corrugation [25]. The surface deformation, especially corrugation, is usual for dirty roads under dry weather conditions; however, ripples also occur on the paved surfaces where traffic does intensive braking or acceleration. This is typical for vertical road curves near intersections.

The decomposition processes and overall quality deterioration of gravel pavement are more difficult to characterise than those observed in asphalt, concrete, or cobbles road pavements. During dry climatic periods, due to the interaction of wheels with the road surface, the pavement wear rises its dustiness, thus negatively impacting the comfort and health of the inhabitants accessing and using this particular type of road [26,27]. On the contrary, rainwater washes away the materials used for reducing dustiness. Also, rainwater washes away fine particles from the pavement surface, weakens the bedrock and results in an increased number of defects and deeper tracks on gravel pavements [28].

Defects of the gravel pavement causes the decrease of driving speed, comfort and friction [29,30], intensify vehicle chassis damage [31]. Wavelength and the spatial frequency of road pavement characterise irregularities and a texture effect on vehicle response. Vehicle components wear, rolling resistance and discomfort properties are sensitive to longer wavelengths (unevenness and partly mega-texture), while friction between the tyre and the road interacts at mega, macro and micro-texture levels. Moreover, two types of pavement profile waves are specified at the size of the tyre-asphalt contact area: short waves are 3–6 mm in length, and long waves are 20–30 mm [32]. This particular research demonstrates that the 1 mm maximum height of micro-irregularities has been found until adhesion tends to increase; however, this regularity is not applicable for rough surfaces.

Different maintenance procedures, including mainly light or hard blading, sand cushioning, reshaping, re-gravelling, etc., are applied for the gravel pavement [33]. Bitumen emulsion spraying is used as an effective method for decreasing dustiness [34]. Jurkevičius et al. [35] defined the road maintenance management system based on the prediction of pavement performance and deterioration models. The model applied for gravel pavements calculates the gravel loss of thickness [36]. It enables to plan gravel layer's thickness for road rehabilitation or a new road. Data on traffic, climate and roughness variation, material quality, gradeability and cost should be collected to select an optimal road maintenance strategy.

Pavement quality evaluation, including roughness measurements, should be made to plan the road pavement maintenance. Various methods and devices are used for evaluating the roughness and deterioration level of the road pavement [37,38]. For profiling, various devices as a straightedge, a dipstick, the Merlin machine and an inertial profiler are commonly used [39,40]. Response based devices (displacement or acceleration sensors, equipped trailers or vehicles) are widely applied due to fast processing and low-cost equipment available [41,42,43,44,45,46,47]. Monitoring the state and quality of the unpaved roads can be based on visual observations and in-person surveying, contrary to paved road evaluation when data are collected automatically [48]. The digital image acquisition system was applied to utilise the unmanned aerial vehicle (UAV); however, limited pavement distresses were captured (mainly potholes and rutting). The flight range of the UAV makes it widely not-applicable. Ride quality assessment of vehicle response is convenient enough, though the most characteristic driving speed is not the same for different quality pavements. Other various identification principles are also known from the literature, for example, a mechanical profilometer for three-dimensional terrain models [49], smartphone accelerometer processing [50], or image analysis [51], reconstruction methods using additional sensors [52,53].

Various ride quality assessment indicators are defined to describe the impact of road roughness. In the last 15 years, several new indexes were introduced [54]. Loprencipe and Zoccali [55] compared the relation between Ride Number (RN), Michigan Ride Quality

Preprints (www.preprints.org) | NOT PEER-REVIEWED | Posted: 16 July 2021 doi:10.20944/preprints202107.0370.v1

Index (RQIMich), Minnesota Ride Quality Index (RQIMn) and frequency-weighted vertical acceleration (a_{wz}) and their relationship with the most-used IRI. The RN, RQIMich and RQIMn have been developed considering road customer opinions, and their thresholds of ride quality level are not speed-related. Therefore, the weighted acceleration a_{wz} provided by ISO 2631 [56] is applicable for lower speed roads (not exceeding 50 km/h). Gurmail and Kiss [57] analysed the response of towed vehicle construction employing the Power Spectral Density (PSD) function to determine the effect of vehicle wheel-ground interaction on structural deterioration. Different types of roads having high and low-quality surfaces were selected before simulation analysis. The same frequency ranges with the elevated local maximum of the PSD characteristic increasing speed from 3.6 to 18 km/h were determined for a rough gravel road. The conducted research also states that under low speed towed vehicle conditions (up to 20 km/h), micro-obstacles (humps and holes) occur with shorter than 2.4 m of wavelength or greater than 0.4–1 m wave numbers on agricultural roads. A smooth exponential increase in root means square (RMS) values of the measured accelerations in the speed range from 3.6 to 25 km/h was determined. Lower surface quality roads having the irregular forms of roughness are not suitable for the conventional IRI based-description, despite its broad applicability and simple enough computational implementation [58]. Different values of other indicators (for passengers in particular) were determined for the roads with the same IRI values; therefore, alternative roughness or vehicle/passenger response indicators (as RMS of accelerations) can be used for specific pavements. Some significant aspects of comfort evaluation in the cabins of different bus topologies were also highlighted in the content of IRI limitation [59]. First, it was argued that the case of close IRI values was possible for three different road profiles and that passengers would experience different vibration conditions. Then, insufficient sensitivity to lateral motions (acceleration) based on experimental data was proved. Due to the limited IRI evaluation of the specific or unpaved road surface, dynamic response-based devices or road profile scanners were being used [45]. On-vehicle added devices show a high enough correlation with the IRI and allow real-time measurement.

Road infrastructure in different regions is developed unevenly as there are a large number of gravel coatings in suburban and rural areas. The majority of research works of vehicle-road interaction focus on asphalt pavement; however, gravel roads condition evaluation is commonly performed using methodologies developed several decades ago, so new solutions are needed.

3. Indexes for Gravel Road Quality Assessment

The fundamental concept of road surface profiles at different mechanical vibration levels is described in international standard ISO 8608 [60]. The PSD of vertical road profile displacement $G_d(n)$ or its rate of change by velocity $G_v(n)$ or acceleration $G_a(n)$ conforming to spatial frequency (n) are used for defining the degree of roughness:

$$G_d(n) = G_d(n_0)\left(\frac{n}{n_0}\right)^{-w}, \quad (1)$$

$$G_v(n) = (2\pi n)^2 \cdot G_d(n), \quad (2)$$

$$G_a(n) = (2\pi n)^4 \cdot G_d(n), \quad (3)$$

where n – spatial frequency (cycles/m), n_0 – reference spatial frequency (0.1 cycles/m), w – pavement waviness indicator, or the exponent of the fitted PSD. For general use, the road roughness indicator usually takes the values of $1.75 < w < 2.25$ [61] and for ISO classification assuming constant velocity PSD, $w = 2$.

The gravel pavement profile cannot be approximated with the waviness of w = 2 used in ISO 8608, which usually occurs on paved roads [46]. Múčka [62] reviewed that up to 40% of roads had differences in wavebands, and 20% of sections had short wave une-

Preprints (www.preprints.org) | NOT PEER-REVIEWED | Posted: 16 July 2021 doi:10.20944/preprints202107.0370.v1

venness ($w > 2$). Another type of specific road usually used for evaluating vehicle dynamics is known as Belgian paving also has few brakes in its displacement spectral density characteristic [63]. There the wavenumber of 6 cycles/meter corresponds with the size of cobbles forming the pavement [64].

Generally, PSD expresses power in a signal per unit frequency [65]. The PSD of road profile displacement is also expressed by unevenness index C [66]:

$$G_d(n) = C \cdot n^{-w}. \tag{4}$$

Wavelength λ (m) has an inverse value of spatial frequency. In the time domain, frequency is expressed as the ratio between wavelength and vehicle speed v (m/s), which generally satisfies conditions for light vehicles [67,68]:

$$0.5 \text{ Hz} < \frac{v}{\lambda} < 15 \text{ Hz} \tag{5}$$

In the context of vehicle dynamics and vibration response analysis, it is more convenient to convert excitation from road pavement spatial frequency n (cycles per meter) to temporal frequency f (cycles per second or Hz). In this case, the supposed vehicle speed is involved [69]:

$$f = n \cdot v. \tag{6}$$

Then, the PSD of the road pavement, in consonance to temporal frequency $G_d(f)$, is adapted to vehicle speed:

$$G_d(f) = \frac{G_d(n)}{v}. \tag{7}$$

The IRI is the most frequently used single-number indicator usually implemented in road maintenance management plans, ride comfort or stability assessment. The IRI value is estimated from the reference quarter car model, also known as the Golden car model [39], driving at 80 km/h and using two components as the velocity of suspension displacement [70,71]:

$$\text{IRI} = \frac{1}{L}\int_0^{L/v} |\dot{z}_{sm} - \dot{z}_{usm}| dt, \tag{8}$$

where: L – the length of the evaluated road profile (m), v – longitudinal vehicle speed applied for the quarter car model (m/s), $\dot{z}_{sm}$– the velocity of sprung mass (SM) vertical displacement (m/s), $\dot{z}_{usm}$– the velocity of unsprung mass (USM) vertical displacement (m/s), dt – time increment (s).

The Dynamic Load Coefficient (DLC) is used for evaluating vehicle response to ride safety and driving stability and it shows variations in the vertical tyre force comparing with its static force [72,73]:

$$\text{DLC} = \frac{\text{RMS}_{Fz,\text{dyn}}}{F_{\text{stat}}}, \tag{9}$$

where: F_{stat} – static force; $\text{RMS}_{Fz,\text{dyn}}$ – the root mean square of the dynamic vertical tyre force ($F_{z,\text{dyn}}$) determined applying vehicle model simulation or using the formula:

$$F_{z,\text{dyn}} = k_t(z_{usm} - h), \tag{10}$$

where: k_t – tyre radial stiffness (taken from the Golden car model), z_{usm} – vertical displacement of USM, h – the vertical roughness of the road pavement.

The DLC value usually ranges from 0.05 to 0.3, ride safety is high when DLC < 0.1. In contrast, the value above 0.15 is related to shaking wheel interaction with the rough pavement and an increase in contact loss [74].

4. Roughness Measurement Using Straightedge

Preprints (www.preprints.org) | NOT PEER-REVIEWED | Posted: 16 July 2021 doi:10.20944/preprints202107.0370.v1

The straightedge method from pavement rut depth measurement [75] was selected to collect data collection from the real gravel pavement. The proposed static method is based on measuring the gap between the road surface and the constant length (3.0 m) beam placed along with the track corresponding to the vehicle's left-side wheels. In this research, the straightedge method for measuring the gravel pavement's longitudinal roughness was adopted, which is usually characterised by larger roughness. Therefore, a small correction in measurement was made by adding 20 mm height spacers (h_{spacer}) at the ends of the beam (Fig. 1). An additional spacer was used in the cases when the end of the beam was over pavement dent.

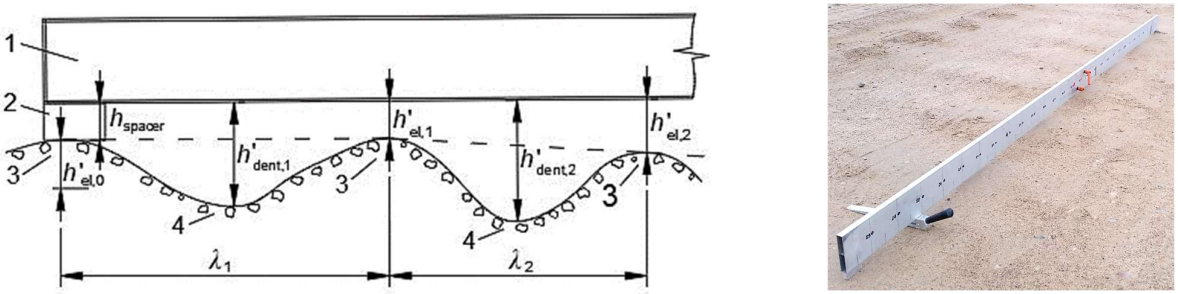

(**a**) (**b**)

Figure 1. The measurement of gravel road roughness applying a straightedge: (a) measurement scheme 1 – straightedge of 3 meters in length; 2 – added spacer; 3 – pavement elevation; 4 – pavement dent; (b) measurement of gravel pavement.

The actual height of elevation and dent is determined by subtracting added spacer height (20 mm) considering each measured vertical distance, which is the clearance between the bottom of the straightedge and the pavement surface at corresponding elevation and dent:

$$h_{\text{el}} = h'_{\text{el}} - 20, \tag{11}$$

$$h_{\text{dent}} = h'_{\text{dent}} - 20, \tag{12}$$

where: h'_{el}, h'_{dent} – the measured height of elevation and dent respectively (mm), h_{el} – the actual height of elevation or clearance between the bottom of the straightedge and the pavement at corresponding elevation (mm), h_{dent} – the actual depth of dent or clearance between the bottom of the straightedge and the pavement at corresponding dent (mm).

The first stage of data post-processing included the inversion of data on the measured pavement elevation. Thus, the negative values of pavement dent were obtained. The absolute depth (amplitude) of the first wave Δ_{λ_1} (Fig. 1), meaning the difference between dent depth and the average of neighbouring elevations, is expressed by the formula**:**

$$\Delta_{\lambda_1} = h_{\text{dent},1} - \frac{h_{\text{el},0} + h_{\text{el},1}}{2}. \tag{13}$$

The absolute depth (amplitude) of the second and next waves:

$$\begin{aligned} \Delta_{\lambda_2} &= h_{\text{dent},2} - \frac{h_{\text{el},1} + h_{\text{el},2}}{2}, \\ &\vdots \\ \Delta_{\lambda_N} &= h_{\text{dent},N} - \frac{h_{\text{el},N-1} + h_{\text{el},N}}{2}. \end{aligned} \tag{14}$$

A straight section of 160 meters long rural road with gravel pavement was selected for this research. Pavement roughness was measured considering the different state of the

 doi:10.20944/preprints202107.0370.v1

pavement. The first state (Pavement State 1, PS-1) means that the gravel pavement measurement was carried out following two days after pavement maintenance by blading without adding gravel material to the existing road surface. This state corresponds to the best-expected quality and driving conditions. The second state (Pavement State 2, PS-2) is described as a middle-quality gravel road following three weeks after pavement maintenance and the start of intensive road deterioration. The third state (Pavement State 3, PS-3) corresponds to the worst pavement quality when maintenance is expected.

After blading, large grains were observed on gravel's flat surface; however, it does not have a significant influence on vehicle response because of tyre enveloping properties. The formed ripples are noticeable on the surface before the maintenance (worst condition), and almost no individual free grains are found.

5. Results

The processed data on the measured profile elevation conforming to the pavement state in the road section is shown in Fig. 2. The amplitudes do not exceed the elevation value of 20 mm in all pavement states; however, the profiles have noticeable differences described further.

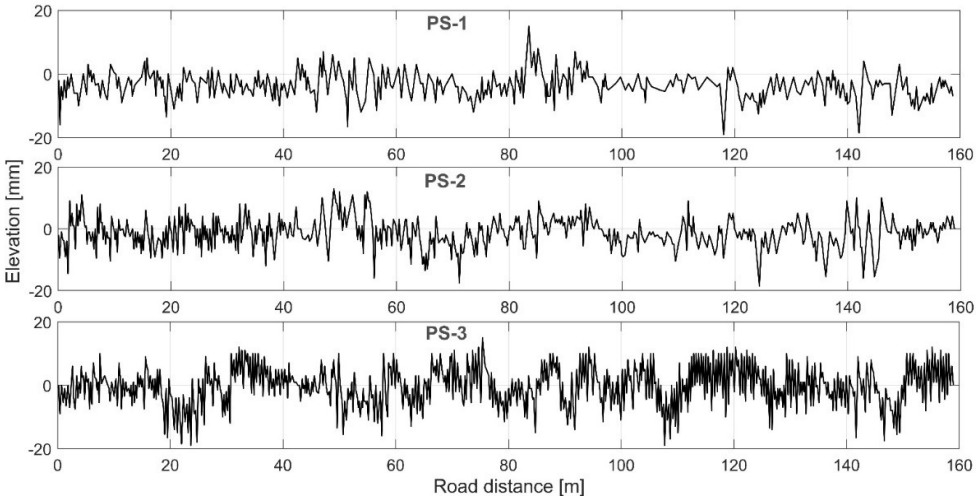

Figure 2. Pavement elevation at the same road section in different pavement states (PS)

The determined surface roughness of the analysed road section is presented in line with ISO 8608 methodology in the form of displacement spectral density – spatial frequency (Fig. 3). The pavement roughness description concerning the PSD log-log plot has a specific break from a smooth characteristic at spatial frequency n = 2 cycles/m (Fig. 3). The characteristic of PS-3 has an additional break at around 6.5 cycles/m. These PSD characteristic slope changes show variations in profile waviness at different bands of waves (long, medium, or short). The corrugation or 'washboard' phenomenon is recognised at the investigated road section. It is the most characteristic for state PS-3, where the shortest waves with the smallest variance are established. Furthermore, the maximum number of the estimated waves represented PS-3, which confirmed the worst quality. Such smooth and constant ripples at certain road sections make driving extremely uncomfortable and unsafe at a specific speed, which is also one of the reasons for pavement corrugation.

Preprints (www.preprints.org) | NOT PEER-REVIEWED | Posted: 16 July 2021 doi:10.20944/preprints202107.0370.v1

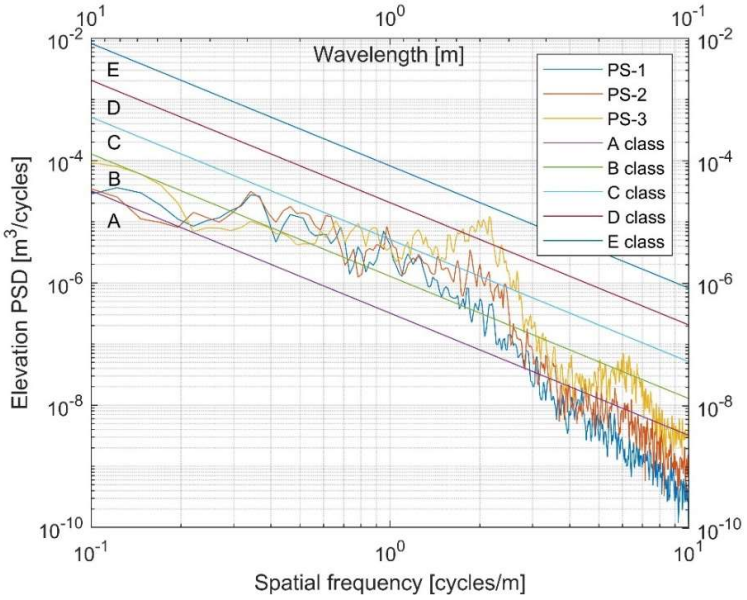

Figure 3. Roughness representation of the measured road section in its different states

The performed analysis of the wavelengths formed on the gravel pavement allows inspecting the reliability of the calculated IRI of the investigated pavement.

5.1. The IRI approach to the gravel pavement

Methodically, the velocities of SM and USM in a vertical direction of the Golden car model are determined and used for calculating the IRI value (Eq. 8). The second column in Table 1 shows the IRI values of the different states of the gravel pavement at a driving speed of 80 km/h, as provided in ASTM [65]. Under the deteriorating road pavement condition, IRI values change inconsistently: the highest IRI value (7.28 m/km) was obtained under pavement condition PS-2, while the lowest value (5.51 m/km) under pavement condition PS-3. This is not in line with the visually observed (Fig. 2) trends in pavement roughness deterioration from PS-1 to PS-3. To analyse the resulting distribution of IRI values concerning the pavement condition, the vertical velocities of SM and USM were calculated. Table 1 shows the calculated RMS of SM and USM velocities in vertical directions, where RMS was calculated as follows:

$$\mathrm{RMS}_{\dot{z}_i} = \left[\frac{1}{T}\int_0^T \dot{z}_i{}^2 \, dt\right]^{1/2}, \tag{15}$$

where: T – the duration of the evaluated road profile (s), i – indicator for the SM or USM depends on the calculated parameter ($\dot{z}_{sm}$ or $\dot{z}_{usm}$).

The values presented in Table 1 show that the RMS of SM velocity increases along with the consistent deterioration of the road pavement condition (from PS-1 to PS-3), but the RMS value of USM velocity is unevenly distributed (as to IRI values). SM movement is inhibited by suspension elements (mainly dampers). At the same time, the USM interacts with the road pavement through the tyre which stiffness (k_t) is around ten times higher than that of suspension (k_s). As a result, the USM moves faster than the SM and has a more significant effect on calculating the IRI. These results indicate that the calculated IRI values are not suitable for analysing the gravel pavements in which the wavelengths of the dominant length in the mega-texture area are formed. Similar results of the higher sensitivity of wheel holder vibrations to the IRI compared with vehicle frame vibrations were captured following the measurements of the reconstructed urban roads with cobblestone and asphalt pavements in [76].

Table 1. The estimated IRI values of the analysed gravel pavement

Preprints (www.preprints.org) | NOT PEER-REVIEWED | Posted: 16 July 2021 doi:10.20944/preprints202107.0370.v1

Pavement State	IRI, m/km	Velocity RMS, m/s	
		SM	USM
PS-1	6.33	0.0283	0.1821
PS-2	7.28	0.0313	0.2303
PS-3	5.51	0.0378	0.1530

The IRI value of the road pavement is determined by simulating a quarter car model as a vehicle moving at a speed of 80 km/h. Due to comfort and sufficient stability, the tested road section of gravel pavement is characterised by lower driving speeds. Therefore, IRI values were calculated for a wider (30–90 km/h) speed range (Fig. 4a). The received IRI values are significantly higher at lower speeds because the same road section is covered over a longer time duration, leading to higher accumulated suspension displacement at IRI calculation. In this case, value distribution at a given speed under a certain road pavement condition rather than the IRI absolute value is analysed. Figure 9a shows that, at lower speeds (30 and 40 km/h), IRI values increase along with the road pavement deterioration from PS-1 to PS-3. At speed above 45 km/h, the distribution of IRI values changes: the values of IRI_{PS-3} corresponding to the worst road condition become lower than the values of IRI_{PS-2}, whereas, at speed above 55 km/h, the value of $IR_{IPS\,3}$ matching to the worst road condition becomes lower than that of IR_{IPS-1} (under the best-quality pavement state). Thus, for calculating the IRI value, a speed of 45–55 km/h meets with the transition phase, the IRI value of which is incorrectly consistent with the pavement condition.

The RMS of the SM and USM velocities was used to analyse IRI values variations (Fig. 4b). Fluctuations in RMS values demonstrated that an increase in driving speed results in minor changes in the SM velocity (continuous lines). However, changes in the velocity of the USM were found to be significant (dotted lines). Also, USM_{PS-3} is on the declining trend as speed increases while USM_{PS-1} and USM_{PS-2} are on the upward trend. These trends in the USM are repeated for IRI values and confirm that a speed of 30–45 km/h is compatible with the pavement state (PS) of the gravel road (Fig. 4a).

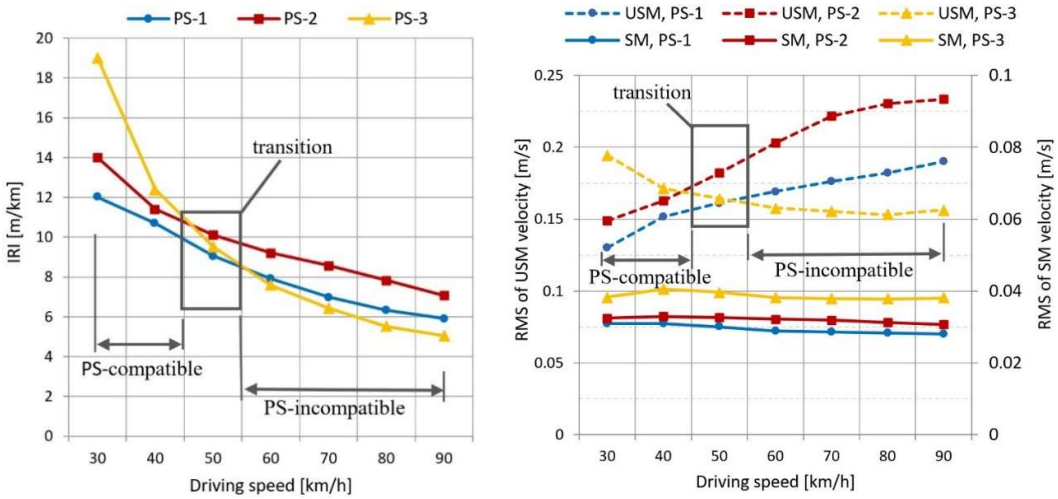

(**a**) (**b**)

Figure 4. The analysis of IRI calculation sensitivity in line with calculation-applicable speed: (**a**) IRI values; (**b**) RMS values of SM and USM displacement velocity.

5.2. Vehicle Response to the Pavement State

Preprints (www.preprints.org) | NOT PEER-REVIEWED | Posted: 16 July 2021 doi:10.20944/preprints202107.0370.v1

In line with ISO 8608, the presented initial characteristic of the measured road roughness (Fig. 3) shows a clear peak of displacement PSD at a spatial frequency of 2 cycles/m for the third pavement state (PS-3). Also, this peak is repeated at six cycles/m of the frequency range. Such unevenness of the characteristic is considerably weakened in the second surface state (PS-2) and is completely invisible under the best (PS-1) state. Converting road roughness characteristics to temporal frequency (Eq. 6, 7) reveals these characteristics' irregularities at different vehicle driving speeds (Fig. 5). The speeds up to 70 km/h are shown, as a higher road speed on the gravel pavement is prohibited under national road traffic regulations. The most pronounced fractures in the elevated PSD are observed for the third surface state PS 3 (Fig. 5): peak for 10 km/h at 5–6 Hz, a peak for 30 km/h at 15–18 Hz, a peak for 50 km/h at 23–30 Hz, a peak for 70 km/h at 33–42 Hz.

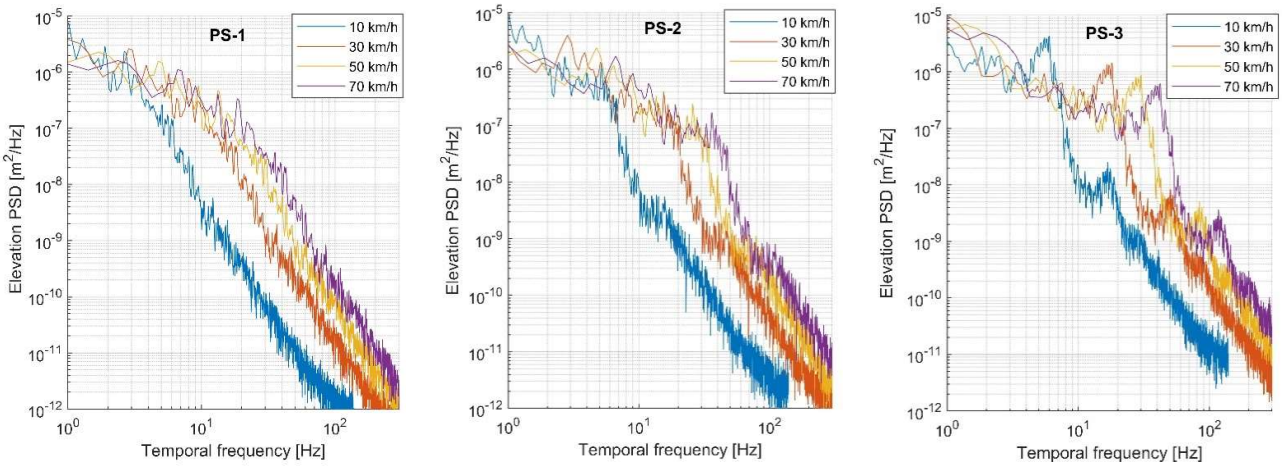

(**a**) (**b**) (c)

Figure 5. Roughness representation in temporal frequency measured at different driving speeds and pavement states: (**a**) PS-1; (**b**) PS-2; (**c**) PS-3.

Driving at lower speeds (10-30 km/h) through short wavelength roughness (PS-3) formed on the gravel pavement (macro-texture level) demonstrates that vibration frequency caused by waves approaches the natural frequency of vehicle USM (11–15 Hz). This order vibration tends to increase the variability in the normal load of the wheel described by the DLC [77,78]. The normal force of the tyre depends on suspension characteristics [79]; however, the road pavement and driving speed has a direct influence. The calculated DLC values for the quarter car model working at a wide speed range (10–90 km/h) are shown in Fig. 6. Here, the Golden car model simulation in MATLAB/Simulink environment was used. Conforming to the pavement state, the obtained DLC values have the same distribution as the IRI (Table 1) due to the dominant movement of the USM (the highest RMS of the USM for PS 2). Both tendencies (IRI and DLC) prove that the second pavement state (PS 2) excites resonant motion for the analysed light car model.

To analyse vehicle response changes in different gravel pavement states, the spectral density of pavement displacement at vehicle vertical dynamics sensitive range of 0–20 Hz was selected (Fig. 7). The excitation of the road pavement to the vehicle driven at a speed of 10 km/h corresponds to an increase in the pavement deterioration level (Fig. 7a). Although there is no significant rise in pavement excitation for SM and USM dynamics at 10 km/h (at 1–2 Hz and 10–14 Hz, respectively), the undesired excitation occurs at the human body sensitive frequency range of 4–8 Hz (ISO 2631-1) on PS 3 and PS 2 pavements. As the speed of 10 km/h is more typical for special purpose vehicle having different suspension and tyre properties, this research on light vehicles application is continued analysing higher speeds.

Preprints (www.preprints.org) | NOT PEER-REVIEWED | Posted: 16 July 2021 doi:10.20944/preprints202107.0370.v1

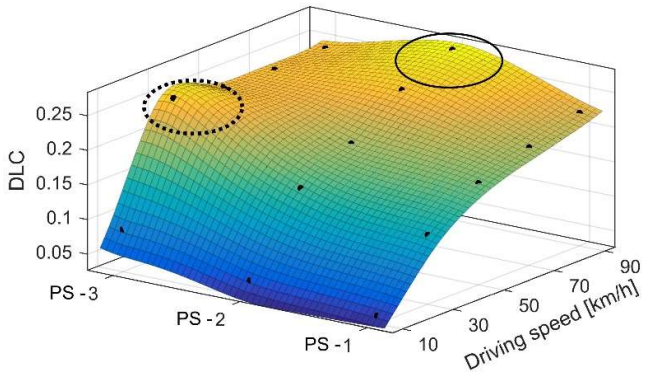

Figure 6. The estimated DLC at different driving speeds and investigated pavement states

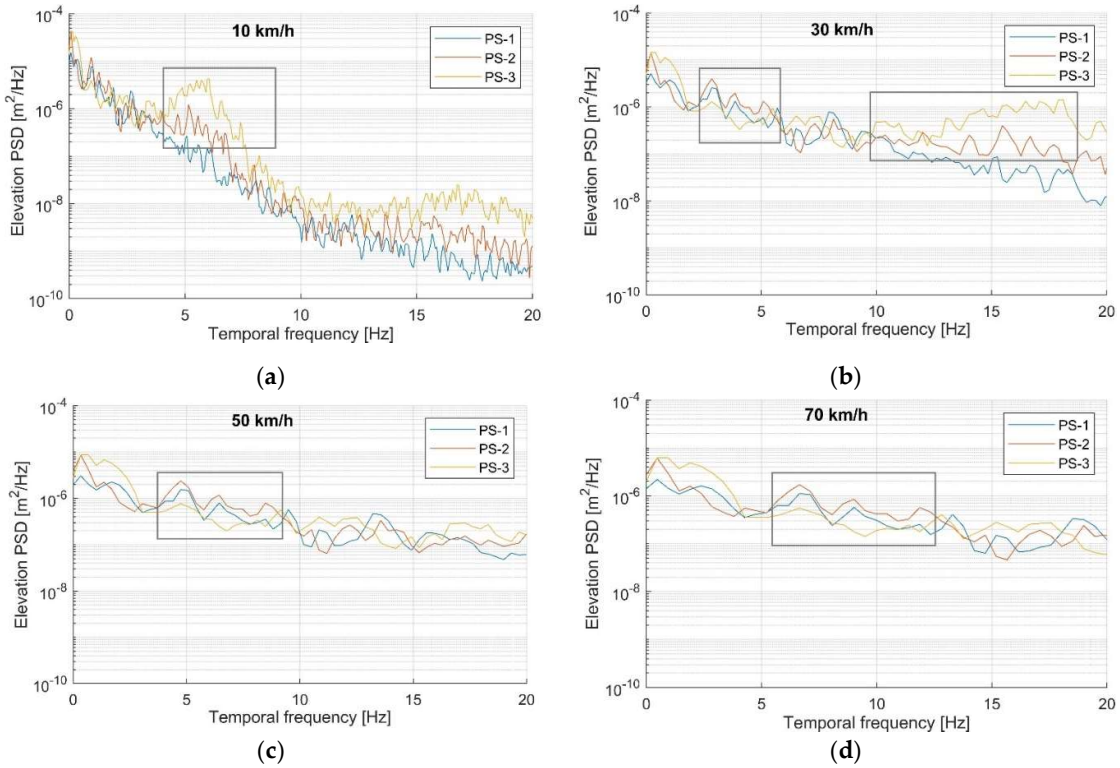

Figure 7. Roughness representation in the temporal frequency: (**a**) 10 km/h; (**b**) 30 km/h; (**c**) 50 km/h; (**d**) 70 km/h

The characteristic of 30 km/h (Fig. 7b) points out two crucial cases. Excitation at a human sensitive frequency range of 2.5–5.5 Hz is higher in the middle-quality pavement state (PS-2) and is the lowest in state PS-3. This also shows that a slightly higher driving speed (from 10 km/h) makes a milder impact on the human body. The second important point in the case of 30 km/h indicates the exclusively high excitation of pavement PS-3 at a frequency range of 10–18 Hz. This frequency range covers the resonant frequency of the USM and increases variability in the dynamic tyre force, contact loss, and vehicle chassis wear. The corresponding peak of the DLC characteristic is marked with the dotted line (Fig. 6). The conversion of PS 3 characteristics from the lowest position at 2.5–5.5 Hz to the highest at 10–18 Hz (Fig. 7b) shows the possible erroneous driver's sensation about comfortable enough driving, but an imperceptible decrease in road holding.

The characteristics of the speeds of 50 km/h and 70 km/h do not have distinguished peaks or rises (Fig. 7c and 7d). However, the above introduced two characteristics have

Preprints (www.preprints.org) | NOT PEER-REVIEWED | Posted: 16 July 2021 doi:10.20944/preprints202107.0370.v1

the same feature of higher PS-2 excitation in the middle-frequency range: 4–9 Hz for 50 km/h and 5.5–12.5 Hz for 70 km/h. The difference between these two cases is that excitation corresponding to 50 km/h affects the human body, while excitation corresponding to 70 km/h additionally affects USM dynamics (wheel contact). The latter is also recognised at the DLC characteristic (marked with the continuous line in Fig. 6).

Excitation at a low-frequency range of 1–2 Hz sensitive for driving comfort is higher on the PS-3 road, but this is reasonable because it is the worst quality pavement.

In general, all PSD curves of pavement excitation tend to descend with each increase (Fig. 7). This may lead to a false perception that a higher speed on the gravel pavement gives better driving comfort or safety. The individual analysis of different operating frequencies allowed distinguishing vehicle stability, comfort and human body sense. Lower pavement excitation for specific frequencies causes better comfort, but the individual cases of a high DLC warn about the potential of vehicle stability loss.

Natural frequencies utilising the quarter car model's damping ratios (Golden car parameters [39]) were determined from the Bode plot (Fig. 8a). Natural frequencies were placed into the speed-wavelength-frequency characteristic (Fig. 8b), showing sensitive frequencies overlapping pavement wavelengths at a specific driving speed. The characteristic shows that SM (vehicle body) vibration is amplified by the pavement with the dominant wavelength of 2–30 m at the driving speed in the range of 10–130 km/h, while USM vibration (wheels and axles) will be amplified by the wavelengths of 0.25–3.5 m in length (Fig. 8b).

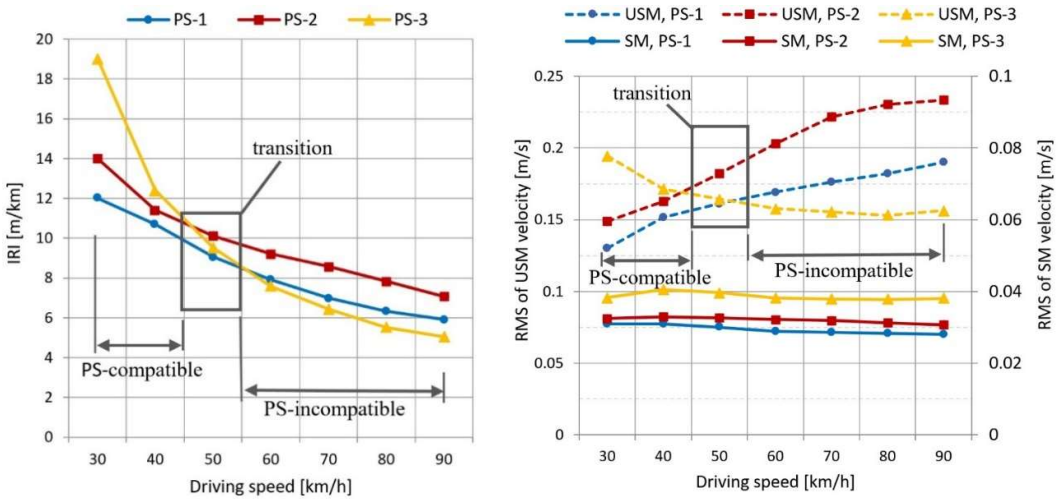

(**a**) (**b**)

Figure 4. The analysis of IRI calculation sensitivity in line with calculation-applicable speed: (**a**) IRI values; (**b**) RMS values of SM and USM displacement velocity.

For example, a usual highway asphalt pavement and the unevenness of 10 m wavelength cause uncomfortable driving at around 30–50 km/h (speed curves cross the solid black line in Fig. 8b). However, this speed is not characteristic of highway driving, and thus a hardly deteriorated pavement prevents discomfort. Vehicle instability caused by wheel resonance under such conditions is barely activated as the natural frequency of the USM (wheel hop) does not cross any speed curve at the above mentioned 10 m wavelength. On the contrary, the second example presents unpaved roads with gravel pavement where short wavelengths dominate. Considering the 1 m wavelength, the natural frequency of SM is not reached (solid line in Fig. 8b). However, the USM resonances at a speed range of 30–50 km/h (crosses dotted line), thus causing unstable wheel contact with the pavement. Shorter wavelengths activate USM resonance at a lower driving speed. Furthermore, the human body sensitive frequency range of 4–8 Hz falls into the short-middle

 doi:10.20944/preprints202107.0370.v1

wavelength band (0.3–5 m) for a wide range of speeds. The obtained vibrations correspond to uncomfortable and unstable driving at specific road pavement waviness for a certain speed.

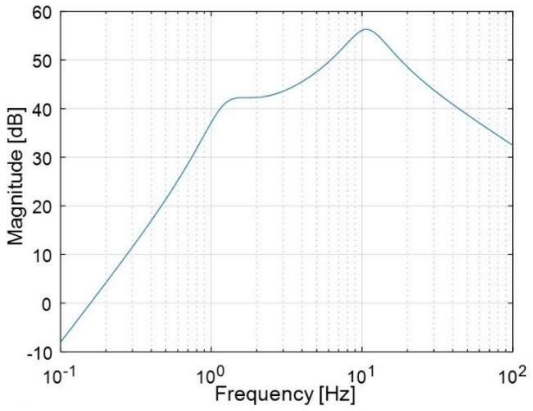

Vehicle mode shape	Natural frequency, ω_n, Hz	Damping ratio, ζ
SM bounce	1.17	0.33
USM vertical hop	10.75	0.30

(**a**)

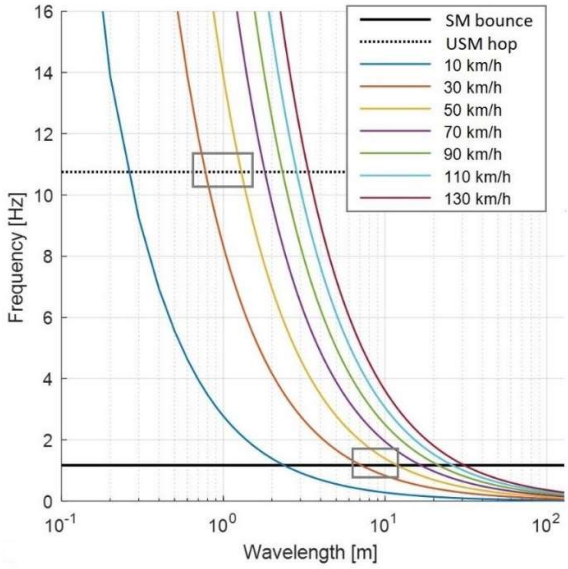

(**b**)

Figure 8. Sensitive vehicle frequencies of pavement wavelengths: (**a**) – natural frequencies and damping ratios of the Bode plot; (**b**) – wavelength frequency characteristics conforming to driving speed.

In this Section, it was proved that the IRI index could be used to evaluate the gravel road pavement condition; however, the significant proposal to calculate the index using the specific velocity interval from 30 to 45 km/h for gravel pavement was indicated. PSD and DLC indexes with frequency response characteristics provide valuable information about the impact of different road roughness levels on discomfort and safety at a certain driving speed.

6. Conclusions

The study aimed to determine changes in the quality of the gravel pavement overtime during road service life in line with the level of surface roughness and pavement excitation on vehicle response and driving comfort. The roughness of the experimental 160 m long section road with gravel pavement was measured continuously three times by adopting the 3 m straightedge method: (1) two days after pavement maintenance (blading), (2) three weeks after pavement maintenance and (3) assessing the worst pavement quality before maintenance. Measurement results showed the continuous deterioration of the investigated road quality under an increase in pavement roughness. Pavement elevation spectral density disclosed several fractures in the roughness log-log plot, which means variations in pavement waviness. For the worst road pavement quality (PS-3), the dominance of the short waves of approximately 0.5 m in length was found (lowest standard deviation), which is compatible with the corrugation phenomenon of the transverse ripples formed. Furthermore, such a wavy pattern has been found to cause the unsprung mass (USM) resonant excitation of the vehicle before the worst road quality is achieved.

Spatial frequency conversion to temporal was done to analyse vehicle dynamics response at different driving speeds. Although the specific fractures of surface power spectral density (PSD) characteristics remained, for the worst quality pavement state, in particular, speed-affected frequencies have shifted to higher bands. Speed is mostly related

to driving safety, and therefore the dynamic load coefficient (DLC), as the indicator of tyre-pavement interaction and vehicle stability, was determined considering the analysed pavement states. Even quarter car simulations of driving at a low speed (< 30 km/h) showed that the DLC reached values higher than 0.15 but did not exceed the value of 0.3 when the proportion of wheel contact loss grew rapidly. However, the DLC undesirably increases at a low speed of 30 km/h on the worst quality pavement and a high speed of 90 km/h on the middle-quality pavement. Even though most countries have a speed limit of 70 km/h on gravel pavements, a potential wheel contact force loss draws attention to timely road maintenance. Variations in driving comfort sensation and the indirect prediction of wheel pavement interaction complicate the driver's selection of safe driving speed. Therefore, vehicle active chassis systems should be continuously developed for better performance on a specific road as variable roughness gravel pavement.

In consonance with the estimated vehicle suspension response to the investigated type of the gravel pavement, IRI values have been scarcely found to correspond to the actual level of pavement roughness. Therefore, this worldwide-spread single-number indicator used for road maintenance planning is not appropriate for the unpaved pavements with unsteady waviness. Absolute IRI values do not provide reliable results that can be used for safe speed estimation. However, calculating the IRI at a speed range of 30–45 km/h shows an increase in the values corresponding to the deteriorating pavement state. Thus, the IRI values calculated at a low speed (30 km/h) are suitable for assessing the gravel pavement condition and road maintenance planning.

The achieved results can be used by operators ensuring road quality and researchers for the decision making about road maintenance, analysing the effect of the unpaved road on vehicle driving stability, comfort, active safety systems performance, drivers and road maintenance planners and supervisors.

The future experimental and theoretical research will focus on vehicle dynamic response measurements and driver comfort evaluation in different driving modes under varying pavement states. Continuous research will also cover higher-order frequency bands related to the issues of tyre dynamics and active vehicle safety control over driving on unpaved roads. The development of pavement roughness measurement utilising laser sensors and artificial intelligence-based image analysis for pavement state identification is planned. The results of direct roughness measurements and their analysis presented in this study will also work for validation of further research.

Author Contributions: Conceptualization, V.Ž. and H.S.; methodology, V.Ž and H.S; software, V.Ž. and E.Š.; validation, V.Ž., V.I. and V.S.; formal analysis, V.Ž.; investigation all authors; resources, V.S.; data curation, E.Š and V.Ž.; writing—original draft preparation, all auhors ; writing—review and editing, V.Ž, E.Š. and V.I.; visualization, V.Ž.; supervision, V.S.. All authors have read and agreed to the published version of the manuscript.

Funding: This research was funded from the European Union Horizon 2020 Framework Program, Marie Skłodowska-Curie actions, under grant agreement No. 872907.

Data Availability Statement: Data available by request from vidas.zuraulis@vilniustech.lt

References

1. Horiuchi, S.; Tsuda, A.; Kobayashi, H.; Redding, C.A.; Prochaska, J.O. Sustainable transportation pros, cons, and self-efficacy as predictors of 6-month stage transitions in a Chinese sample. *J Transp Health* **2017**, *6*, 481–489, doi:10.1016/j.jth.2017.05.363.
2. Obeng, D.A.; Tuffour, Y.A. Prospects of alternative funding sourcing for maintenance of road networks in developing countries. *Transp Res Interdiscip Perspect* **2020**, *8*, 100225:17, doi:10.1016/j.trip.2020.100225.
3. Pasindu, H.R.; Gamage, D.E.; Bandara, J.M.S.J. Framework for selecting pavement type for low volume roads. *Transp Res Proc* **2020**, *48*, 3924-3938, doi:10.1016/j.trpro.2020.08.028.
4. Petkevičius. K.; Maskeliūnaitė, L.; Sivilevičius, H. Determining travel conditions on motorways for automobile transport based on the case study for Lithuanian highways. *Transport* **2019**, *34(1)*, 89–102, doi:10.3864/transport.2019.7842.
5. Ziyadi, M.; Ozer, H.; Kang, S.; Al-Qadi, I.L. Vehicle energy consumption and an environmental impact calculation model for the transportation infrastructure systems. *J Clean Prod* **2018**, *174*, 424–436, doi:10.1016/j.jclepro.2017.10.292.

6. European Parliament. EU Road Surfaces: Economic and Safety Impact of the Lack of Regular Road Maintenance. External authors Frisoni, R.; Dionori F.; Casullo L.; Vollath, C.; Devenish, L.; Spano, F.; Sawicki, T.; Carl, S.; Lidia, R.; Neri, J.; et al.. A. Study. Structural and Cohesion Policies: Transport and Tourism; **2014**.
7. Mamčic, S.; Sivilevičius H. The analysis of traffic accidents on Lithuanian regional gravel roads. Transport. **2013**, *28(1)*, 108–115, doi:10.3846/16484142.2013.782894.
8. Pretagostini, F.; Ferranti, L.; Berardo, G.; Ivanov, V.; Shyrokau, B. Survey on Wheel Slip Control Design Strategies, Evaluation and Application to Antilock Braking Systems. *IEEE Access* **2020**, *8*, 10951–10970, doi:10.1109/access.2020.2965644.
9. van der Merwe, N.A.; Els, P.S.; Žuraulis, V. ABS braking on rough terrain. *J Terramech* **2018**, *80*, 49–57, doi:10.1016/j.jterra.2018.10.003.
10. Cao, D.; Song, X.; Ahmadian, M. Editors' perspectives: road vehicle suspension design, dynamics, and control. *Veh Syst Dyn* **2011**, *49(1-2)*, 3–28, doi:10.1080/00423114.2010.532223.
11. Hamersma, H.A.; Els, P.S. Improving the braking performance of a vehicle with ABS and a semi-active suspension system on a rough road. *J Terramech* **2014**, *56*, 91–101, doi:10.1016/j.jterra.2014.09.004.
12. Šabanovič, E.; Žuraulis, V.; Prentkovskis, O.; Skrickij, V. Identification of Road-Surface Type Using Deep Neural Networks for Friction Coefficient Estimation. *Sensors* **2020**, *20(3)*, 612, doi:10.3390/s20030612.
13. Žuraulis, V.; Surblys, V.; Šabanovič, E. Technological measures of forefront road identification for vehicle comfort and safety improvement. *Transport* **2019**, *34(3)*, 363-372, doi:10.3846/transport.2019.10372.
14. Savitski, D.; Ivanov, V.; Shyrokau, B., De Smet, J.; Theunissen, J. Experimental study on continuous ABS operation in pure regenerative mode for full electric vehicle. *SAE Int. J. Passeng. Cars-Mech. Syst* **2015**, 8(1), 364-369, doi.org/10.4271/2015-01-9109.
15. Gao, H.; Jézéquel, L.; Cabrol, E.; Vitry, B. Chassis durability and comfort trade-off at early stage of project by virtual proving ground simulation. *Veh. Syst Dyn* **2021**, 5–20, doi:10.1080/00423114.2021.1896011.
16. Fauriat, W; Mattrand, C.; Gayton, N.; Bekou, A.; Cembrzynski, T. Estimation of road profile variability from measured vehicle responses. *Veh Syst Dyn* **2016**, *54(5)*, 585–605, doi:10.1080/00423114.2016.1145243.
17. Kerst, S.; Shyrokau, B.; Holweg, E. Anti-lock braking control based on bearing load sensing. *Proc. EuroBrake* **2015**, 4–6.
18. Vantsevich, V. V.; Shyrokau, B. N. Autonomously operated power-dividing unit for driveline modeling and AWD vehicle dynamics control. *In Dynamic Systems and Control Conference* **2008**, 43352, 891–898, doi:10.1115/DSCC2008-2224.
19. Bitelli, G.; Simone, A.; Girardi, F.; Lantieri, C. Laser Scanning on Road Pavements: A New Approach for Characterizing Surface Texture. *Sensors* **2012**, 12, 9110–9128, doi:10.3390/s120709110.
20. ISO 13473-2: 2002 Characterisation of pavement texture by use of surface profiles – Part 2: Terminology and basic requirements related to pavement texture profile analysis. Geneva, Switzerland: International Standardization Organization; **2002**.
21. Walker, D.; Entine, L.; Kummer, S. Pavement Surface Evaluation and Rating (PASER) Manual. Gravel Roads. Wisconsin Transportation Information Center, University of Wisconsin-Madison; **2002**.
22. Kropáč, O.; Múčka, P. Deterioration Model of Longitudinal Road Unevenness Based on its Power Spectral Density Indices. *Road Mater Pavement Des* **2008**, *9(3)*, 389–420, doi:10.1080/14680629.2008.9690125.
23. Taberlet, N.; Morris, S.W.; McElwaine, J.N. Washboard Road: The dynamics of granular ripples formed by rolling wheels. *Phys Rev Lett* **2007**, *99*, 068003, doi:10.1103/PhysRevLett.99.068003.
24. Both, J.A.; Hong, D.C.; Kurtze, D.A. Corrugation of roads. *Physica A Stat Mech Appl* **2001**, *301(1–4)*, 545–559, doi:10.1016/S0378-4371(01)00425-3.
25. Mahgoub. H; Bennett, C; Selim A. Analysis of factors causing corrugation of gravel roads. *Transp Res Rec* **2011**, *2204*, 3–10, doi:10.3141/2204–01.
26. Edvardsson. K; Magnusson, R. Monitoring of dust emission on gravel roads: Development of a mobile methodology and examination of horizontal diffusion. *Atmos Environ* **2009**, *43*, 889–896, doi:10.1016/j.atmosenv.2008.10.052.
27. Zhu, D.; Gillies, J.A.; Etyemezian, V.; Nikolich, G.; Shaw, W.J. Evaluation of the surface roughness effect on suspended particle deposition near unpaved roads. *Atmos Environ* **2015**, *122*, 541–551, doi:10.1016/j.atmosenv.2015.10.009.
28. McClelland, D.E.; Foltz, R.B.; Falter, M.C.; Wilson, W.D.; Cundy, T.; Schuster, R.L.; Saurbier, J.; Rabe, C.; Heinemann, R. Relative Effects on a Low-Volume Road System of Landslides Resulting from Episodic Storms in Northern Idaho. *Transp Res Rec: Transp Res Board* **1999**, *1652(1)*, 235–243, doi:10.3141/1652–63.
29. Uys, P.E.; Els, P.S.; Thoresson, M. Suspension settings for optimal ride comfort of off-road vehicles travelling on roads with different roughness and speeds. *J Terramech* **2007**, *44(2)*, 163–175: doi:10.1016/j.jterra.2006.05.002.
30. Scholtz, O.; Els, P.S. Tyre rubber friction on a rough road. *J Terramech* **2021**, *93*, 41-50, doi:10.1016/j.jterra.2020.11.002.
31. Farrahi, G.H.; Ahmadi, A.; Kasyzadeh K.R. Simulation of vehicle body spot weld failures due to fatigue by considering road roughness and vehicle velocity. Simul Model Pract Theory **2020**, *105*, 102168, doi:10.1016/j.simpat.2020.102168.
32. Raslavičius, L., Pakalnis, A., Keršys, A.; Skvireckas, R.; Juodvalkis, D. Investigation of asphalt texture roughness on friction evolution for wheeled vehicles. *Transport* 2016, *31(2)*, 133–141, doi:10.3846/16484142.2016.1189960.
33. Van Zyl, G. Blading optimisation. Reverting from Theory to Practice. *Transp Res Rec* **2011**, *2204(1)*, 11–20, doi:10.3141/2204-02.
34. Žilionienė, D.; Čygas, D.; Juzėnas, A.A.; Jurgaitis, A. Improvement of functional designation of low-volume roads by dust abatement in Lithuania. *Transp Res Rec: Transp Res Board* **2007**, *1989-1(1)*, 293–298. doi:10.3141/1989-34.
35. Jurkevičius, M.; Puodžiukas, V.; Laurinavičius, L. Implementation of Road Performance Calculation Models Used in Strategic Planning Systems for Lithuania Conditions. *The Baltic J Road Bridge Eng* **2020**, *15(3)*, 146–165, doi:10.7250/bjrbe.2020-15.489.
36. Archondo-Callao, R. HDM-4 Road User Cost Model Documentation, Version 1.20, User's Guide. The World Bank; **2009**.

37. Yunusov, A.; Eshkabilov, S.; Riskaliev, D.; Abdukarimov, N. Estimation and evaluation of road roughness via different tools and methods. In Conference Proceedings of Transport Problems **2019**, XI International Scientific Conference At: Silesian University of Technology Faculty of Transport; Poland. 770–784.
38. Tomiyama, K; Kawamura A. Application of lifting wavelet transform for pavement surface monitoring by use of a mobile profilometer. *Int J Pavement Res Technol* **2016**, *9*, 345–353, doi:10.1016/j.ijprt.2016.08.007.
39. Sayers, M.W.; Karamihas, S.M. *The little book of profiling*, University of Michigan, MI; **1998**.
40. Rajkamal, K.; Reddy, T.D.; Rohith, D.; Chowdary, V.; Prasad, C.S.R.K. Performance Evaluation of Gravel Road Sections Sealed with Surface Dressing. *Transp Res Proc* **2019**, *17*, 81–89, doi:10.1016/j.trpro.2016.11.063.
41. Abulizi, N.; Kawamura, A.; Tomiyama, K.; Fujita, S. Measuring and evaluating of road roughness conditions with a compact road profiler and ArcGIS. *J Traffic Transp Eng (Engl. Ed.)* **2016**, *3(5)*, 398–411, doi:10.1016/j.jtte.2016.09.004.
42. Bidgoli, A.M.; Galroo, A.; Nadjar H.S.; Rashidabad, A.G.; Ganji, M.R. Road Roughness measurement using a cost-effective sensor-based monitoring system. *Autom Constr* **2019**, *104*, 140–152, doi:10.1016/j.autcon.2019.04.007.
43. Du, Y.; Liu, Ch.; Wu, D.; Jiang, S. Measurement of International Roughness Index by Using *Z*-Axis Accelerometers and GPS, Hindawi Publishing Corporation. *Math Probl Eng* **2014**, 928980, doi:10.1155/2014/928980.
44. Eshkabilov, S.; Yunusov, A. Measuring and Assessing Road Profile by Employing Accelerometers and IRI Assessment Tools. *Am J Traffic Transp Eng* **2018**, *3(2)*, 24–10, doi:10.11648/j.ajtte.20180302.12.
45. Leitner, B., Decký, M., Kováč, M. Road pavement longitudinal evenness quantification as stationary stochastic process. *Transport* **2019**, *34(2)*, 195–203, doi:10.3846/transport.2019.8577.
46. Pawar, P.R.; Mathew, A.T.; Saraf, M.R. IRI (International Roughness Index): An Indicator Of Vehicle Response. *Mater Today Proc* **2018,** *5*, 11738–11750, doi:10.1016/j.matpr.2018.02.143
47. Žuraulis, V.; Levulytė, L.; Sokolovskij, E. The impact of road roughness on the duration of contact between a vehicle wheel and road surface. *Transport* **2014**, *29(4)*, 431–439, doi:10.3846/16484142.2014.984330.
48. Shtayat, A.; Moridpour, S.; Best, B.; Shroff, A.; Raol, D. A review of monitoring systems of pavement condition in paved and unpaved roads. *J Traffic Transp Eng. (Engl. Ed.)* **2020,** *7(5)*, 629–638, doi:10.1016/j.jtte.2020.03.004.
49. Becker, C.M.; Els, P.S. Profiling of rough terrain. *Int J Veh Des* **2014**, *64(2/3/4)*, 240–261, doi:10.1504/IJVD.2014.058500.
50. Souza, V.M.A. Asphalt pavement classification using smartphone accelerometer and Complexity Invariant Distance. *Eng Appl Artif Intell* **2018**, *74*, 198–211, doi:10.1016/j.engappai.2018.06.003.
51. Botha, T.R.; Els, P.S. Rough terrain profiling using digital image correlation. *J. Terramech* **2015**, *59*, 1–17, doi:10.1016/j.jterra.2015.02.002.
52. Kerst, S.; Shyrokau, B.; Holweg, E. Reconstruction of wheel forces using an intelligent bearing. *SAE International Journal of Passenger Cars-Electronic and Electrical Systems* **2016**, *9*, 196–203, doe: 10.4271/2016-01-0092.
53. Kerst, S.; Shyrokau, B.; Holweg, E. A Model-based approach for the estimation of bearing forces and moments using outer ring deformation. *IEEE Transactions on Industrial Electronics* **2019**, *67*(1), 461–470, doi:10.1109/TIE.2019.2897510.
54. Múčka P. Current approaches to quantify the longitudinal road roughness. *Int J Pavement Eng* **2016**, *17(8)*, 659–679. doi:10.1080/10298436.2015.1011782.
55. Loprencipe, G.; Zoccali, P. Ride Quality Doe to Road Surface Irregularities: Comparison of Different Methods Applied on a Set of Real Road Profiles. *Coatings* **2017**, *7(5)*, 59, doi:10.3390/coatings7050059.
56. ISO 2631-1: 1997 Mechanical vibration and shock – Evaluation of human response to whole-body vibration. Part I: General requirements. Geneva, Switzerland: International Standardization Organization; **1997**.
57. Gurmail, L., Kiss, P. A comparative study of destructive effects resulting from road profile acting on off-road towed vehicles. *J. Terramech* **2019**, *81*, 57–65, doi:10.1016/j.jterra.2018.06.002.
58. Kropáč O, Múčka P. Be careful when using the International Roughness Index as an indicator of road unevenness. *J Sound Vib* **2005,** *287*, 989–1003, doi:10.1016/j.jsv.2005.02.015.
59. Fichera, G., Scionti, M., Garescì, F. Experimental correlation between the road roughness and the comfort perceived in bus cabins. SAE Technical Paper 2007-01-0352. **2007**, https://doi.org/10.4271/2007-01-0352.
60. ISO 8608: 2016 Mechanical vibrations – Road surface profiles – Reported of measured data. Geneva, Switzerland: International Standardization Organization; **2016**.
61. Goenaga B, Fuentes L, Mora O. Evaluation of the methodologies used to generate random pavement profiles based on the power spectral density: An approach based on the International Roughness Index. *Ing e Investig* **2017**, *37(1)*, 49-57, doi:10.15446/ing.investig.v37n1.57277.
62. Múčka P. Road waviness and the dynamic tyre force. *Int J Veh Des* **2004**, *36(2-3)*, 216-232, doi:10.1504/IJVD.2004.005357.
63. Els, P.S.; Theron, N.J.; Uys, P.E.; Thoresson, M.J. The ride comfort vs. handling compromise for off-road vehicles. *J Terramech* **2007**, *44*, 303–317, doi:10.1016/j.jterra.2007.05.001.
64. Ngwangwa, H.M.; Heyns, P.S.; Breytenbach, H.G.A., et al. Reconstruction of road defects and road roughness classification using Artificial Neural Networks simulation and vehicle dynamic responses: Application to experimental data. J Terramech. **2014**, *53*, 1–18, doi:10.1016/j.jterra.2014.03.002.
65. ISO/TS 13473-4: 2008 Characterisation of pavement texture by use of surface profiles – Part 4: Spectral analysis of surface profiles. Technical specification. Geneva, Switzerland: International Standardization Organization; 2008.
66. Múčka, P.; Stein, G.J.; Tobolka, P. Whole-body vibration and vertical road profile displacement power spectral density. *Veh Syst Dyn* **2020**, *58(4)*, 630–656, doi:10.1080/00423114.2019.1595675.
67. Rill, G. *Road vehicle dynamics: Fundamentals and modeling*. CRC Press, Taylor & Francis Group; **2012**.

 doi:10.20944/preprints202107.0370.v1

68. Tyan, F.; Hong, Y.F.; Tu, S.H.; Jeng, W.S. Generation of random road profiles. J Adv Eng. **2009**, *4*, 373–1378.
69. Reza-Kashyzadeh, R.; Ostad-Ahmad-Ghorabi, M.J.; Arghavan, A. Investigating the effect of road roughness on automotive component. *Eng Fail Anal* **2014**, *41*, 96–107, doi:10.1016/j.engfailanal.2013.12.008.
70. ASTM: 2003 Standard Practice for Computing International Roughness Index for roads from longitudinal profile measurement. ASTM E 1926–98: West Conshohocken, PA; **2003**.
71. Sayers, M.W. On the calculation of international roughness index from longitudinal road profile. *Transp Res Rec* **1995,** *1501*, 1–12.
72. Cebon, D. *Handbook of vehicle-road interaction*. CRC Press; Lisse, Netherlands, 1999.
73. Múčka, P. Simulated Road Profiles According to ISO 8608 in Vibration Analysis. *J Test Eval* **2018,** *46(1)*, 405–418, doi:10.1520/JTE20140493.
74. Buhari, R.; Rohani, M.M.; Abdullah, M.E. Dynamic Load Coefficient of Tyre Forces from Truck Axles. *Appl Mech Mater* **2013**, *405–408*, 1900–1911, doi:10.4028/www.scientific.net/AMM.405-408.1900.
75. Wang, D.; Falchetto, A.C.; Goeke, M.; Wang, W.; Li, T.; Wistuba, M.P. Influence of computation algorithm on the accuracy of rut depth measurement. *J Traffic Transp Eng (Engl. Ed.)* **2017**, *4(2)*, 156–164, doi:10.1016/j.jtte.2017.03.001.
76. Lakušić, S., Brčić, D., Tkalčević Lakušić, V. Analysis of Vehicle Vibrations – New Approach to Rating Pavement Condition of Urban Roads. *Promet – Traffic Transp* **2012**, *23(6)*, 485–494, doi:10.7307/ptt.v23i6.183.
77. Múčka, P. Road Roughness Limit Values Based on Measured Vehicle Vibration. *J Infrastruct Syst* **2016,** *23(2)*, 04016029, 1–13. doi:10.1061/(ASCE)IS.1943-555X.0000325.
78. Múčka, P. Proposal of Road Unevenness Classification Based on Road Elevation Spectrum Parameters. *J Tes. Eval* **2016**, *44(2)*, 930–944, doi:10.1520/JTE20150179.
79. Xu, Y., Ahmadian, M. Improving the capacity of tire normal force via variable stiffness and damping suspension system. *J Terramech* **2013**, *50(2),* 121–132, doi:10.1016/j.jterra.2013.03.003.